Journal Pre-proof

Sol-gel Ni-based/γ-Al_2O_3 as efficient catalysts for toluene reforming: Catalytic activity during long-term experiments and in presence of H_2S<!–<ForCover>Claude V, Mahy JG, Douven S, Lohay T, Micheli F, Lambert SD, Sol-gel Ni-based/γ-Al_2O_3 as efficient catalysts for toluene reforming: Catalytic activity during long-term experiments and in presence of H_2S, *Journal of Environmental Chemical Engineering*, doi: 10.1016/j.jece.2020.104528</ForCover>–>

Vincent Claude (Conceptualization) (Methodology) (Investigation), Julien G. Mahy (Investigation) (Writing - original draft), Sigrid Douven (Investigation) (Writing - original draft), Timothée Lohay (Conceptualization) (Methodology) (Investigation), Francesca Micheli (Conceptualization) (Methodology) (Investigation), Stéphanie D. Lambert (Conceptualization) (Methodology) (Investigation) (Writing - original draft) (Supervision) (Funding acquisition) (Project administration)

PII: S2213-3437(20)30877-0

DOI: https://doi.org/10.1016/j.jece.2020.104528

Reference: JECE 104528

To appear in: *Journal of Environmental Chemical Engineering*

Received Date: 29 July 2020

Revised Date: 18 September 2020

Accepted Date: 21 September 2020

Please cite this article as: { doi: https://doi.org/

Sol-gel Ni-based/γ-Al_2O_3 as efficient catalysts for toluene reforming: Catalytic activity during long-term experiments and in presence of H_2S

Vincent Claude[1], Julien G. Mahy[1, 2*]julien.mahy@uclouvain.be, Sigrid Douven[1], Timothée Lohay[1], Francesca Micheli[3], Stéphanie D. Lambert[1]

[1] *Department of Chemical Engineering – Nanomaterials, Catalysis & Electrochemistry, University of Liège, B6a, Quartier Agora, Allée du six Août 11, 4000 Liège, Belgium*

[2] *Institute of Condensed Matter and Nanosciences (IMCN), Université catholique de Louvain, Place Louis Pasteur 1, 1348, Louvain-la-Neuve, Belgium*

[3] *Department of Industrial Engineering, University of L'Aquila, 18 via G. Gronchi, 67100 L'Aquila, Italy*

***Corresponding author:** Julien G. Mahy, Institute of Condensed Matter and Nanosciences (IMCN), Université catholique de Louvain, Place Louis Pasteur 1, 1348, Louvain-la-Neuve, Belgium. E-mail address:.

Graphical absstract

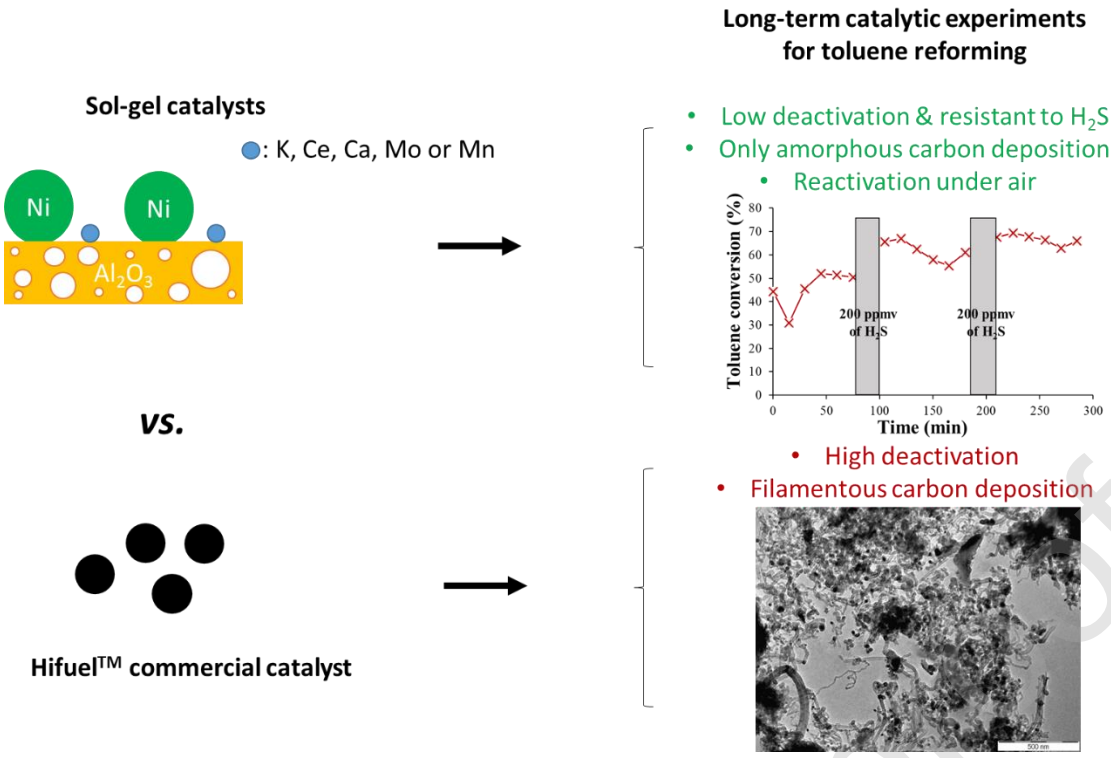

Highlights

- Sol-gel Ni-based/γ-Al_2O_3 catalysts performance on toluene reforming
- Long-term catalytic experiments or under H_2S and comparison with commercial Hifuel™ catalyst
- Low deactivation for sol-gel samples *vs.* high deactivation for Hifuel™
- Easy regeneration of sol-gel materials with unchanged properties and activity
- Sol-gel pure Ni/γ-Al_2O_3 catalyst very resistant to H_2S poisoning

Abstract

Last decades, the valorization of biomass became a topic of interest, and especially the production of syngas by the catalytic reforming of biomass. But one drawback for a large-scale development is the associated production of tars.

This work focuses on the catalytic reforming of tars present in bio-syngas reactors. Efficient Ni-based/γ-Al_2O_3 catalysts were developed in previous studies by an aqueous sol-gel process.

Here, four of those catalysts, exhibiting promising catalytic properties for toluene reforming (used as tar model molecule), were further evaluated on long-term experiments and under H_2S. Indeed, long-term performance and resistance to poisoning are two key properties of catalysts for industrial applications. One commercial catalyst, Hifuel^{TM}, was also evaluated for comparison. The results showed that the pure Ni/γ-Al_2O_3 catalyst presented a low deactivation throughout 30 h of experiment with neither Ni particle size nor support crystallinity alteration. All co-doped Ni/γ-Al_2O_3 catalysts were more resistant against deactivation than the pure Ni/γ-Al_2O_3 catalyst. As only amorphous carbon was deposited, an easy regeneration was performed by heating the catalysts 2 h at 650 °C under air. The catalytic activity remained unchanged in similar 30 h-experiment.

Contrarily, the commercial Hifuel^{TM} catalyst underwent a strong and quick deactivation by the formation of filamentous carbon. The regeneration under air was not sufficient to regenerate the catalyst.

The Ni/γ-Al_2O_3 catalyst activity was assessed in the presence of H_2S. The results showed that the toluene conversion was only slightly affected by the presence of H_2S in the syngas mixture, highlighting its very good resistance to poisoning.

Keywords: Ni/γ-Al_2O_3; toluene reforming; Sol-Gel process; H_2S poisoning; Lifetime of catalyst

1. Introduction

Catalytic reforming is a chemical process widely used to produce useful chemicals from less used products [1–3]. Last decades, some researches focused on the waste valorization, especially on biomass waste [4,5]. Indeed, a syngas, called bio-syngas, could be produced by the catalytic reforming of biomass residues. But the commercial development of such processes is hindered by the production of tars that can clog the reactor and the pipes [4,5]. This work focuses on the catalytic reforming of tars found in bio-syngas reactors. Several catalysts have

been developed for tars reforming [4,6–14]. Interesting catalytic performances (catalytic activity and resistance against deactivation) were reported in literature but they were mostly determined on short experiments, typically 5 h. Very few studies reported the performances during long-term experiments. The lack of such data is problematic since it increases the gap between research results and industrial needs. Indeed, rather than the catalytic activity, the stability of the catalysts is usually the first essential criterion required in industrial applications [12,15]. Actually, during their use, various phenomena (coking, sintering, phase transformation …) potentially damage the catalysts.

The influence of H_2S on the catalytic activity is not always reported in studies related to tars reforming. This lack of information is also generally an obstacle for the use of the catalysts at larger scale. Indeed, H_2S is intrinsically present in the syngas mixture (between 20 and 200 ppmv). H_2S can be removed from syngas by absorbers, specific catalysts [16] or photocatalysts [17–20]. Nevertheless, the operating temperatures require the catalysts for tars removal (primary and secondary) to be used before these purification steps. Therefore, the resistance against H_2S is crucial, especially for secondary catalysts working at low temperatures (500-700 °C) [21]. Indeed, the sensitivity of the reforming catalysts to chemisorbed sulfur compounds is known to increase when the temperature decreases [22]. A good example to illustrate the decisive challenge of developing catalysts resistant to H_2S lies in the study of Gallego *et al.* [23]. The authors developed $LaNiO_3$ perovskite catalysts for the dry reforming of methane exhibiting very good long-term results (100 h without deactivation by carbon). However, only a small amount of H_2S (25 ppm) was sufficient to entirely deactivate the catalyst within 5 h. Other works also detailed the effect of the presence of H_2S on the catalyst activity [22,24–26], leading similarly to catalyst deactivation. Table 1 summarizes the possible global reactions occurring on a metallic active site during catalytic tests in presence of H_2S and during regeneration with H_2O, H_2 or O_2 [21]. In the study of Bassani *et al.*[27], a new process, called

The Acid Gas To Syngas^{TM} (AG2S^{TM}) technology, was applied to the gasification of solid fuel, as biomass, to decrease the H_2S and CO_2 production by increasing the syngas production. The process was mainly described for coal gasification.

In our previous studies [28,29], it has been evidenced that Ni/γ-Al_2O_3 catalysts prepared by sol-gel synthesis showed remarkable stabilities against coke deactivation during 5 h of reaction at 650 °C with 24,000 ppmv of toluene. This high resistance against coking was attributed to a phenomenon called "special reduction with toluene". Due to the exclusive presence of a spinel structure of nickel aluminate ($NiAl_2O_4$) and the operating conditions of the catalytic tests (at the boundary between the oxidation and the reduction of Ni nanoparticles), the molecules of toluene could act as reducing agents. The phenomenon involves the following steps: i) the toluene is adsorbed on NiO and on the alumina support; ii) the toluene molecules are decomposed into carbon (char); iii) NiO and the char react to form $Ni^{(0)}$ and CO_2; iv) CO_2 reacts with the char located at the surface of the support to form CO, which can further reduces the remaining nickel oxides into $Ni^{(0)}$; v) part of the $Ni^{(0)}$ is oxidized back into NiO because of the low operating temperature and the presence of CO_2 and H_2O. This mechanism of autoregeneration was also evidenced by Cheng *et al.* [30]. Nevertheless, in Cheng *et al.* [30], the activity was assessed only for 5 h and no recycling experiment was performed. The doping of Ni-based catalysts is also a good way to enhance the catalytic activity and stability of the catalyst [31]. Among the numerous dopants, Mn, Mo, Ca, K or Ce elements showed interesting catalytic enhancement as pointed out in several studies [32,33], and especially in the case of our Ni/γ-Al_2O_3 catalysts prepared by sol-gel synthesis [34,35].

The aims of this work are to evaluate the performances of such promising sol-gel Ni/γ-Al_2O_3 catalysts (i) during long-term catalytic experiments, (ii) after regeneration of the catalysts and (iii) in the presence of H_2S. The catalytic tests were performed at 650 °C with a standard syngas mixture and with 24,000 ppmv of toluene. The novelty lies in the comprehensive study

combining the evaluation of the catalysts performance over long reaction time even after regeneration and their resistance to H_2S starting from the same promising catalysts. Their properties were studied in relation to the performance to point out the impact of the different types of operating conditions. Even if each type of experiment is reported individually, studies taking into account all the different experiments together are not reported in literature for tars removal. Moreover, a comparison with commercial catalyst is also performed which is often missing in many studies.

In the first part of this study, long-term catalytic experiments were performed for 30 h with the most promising catalysts of our previous studies [34,35] (4 samples). These catalysts were produced by an aqueous sol-gel process [36] and were based on a Ni active phase deposited on γ-Al_2O_3 co-doped with Mn, Mo, Ca, K or Ce. In order to evaluate the performances of the catalysts, a commercial steam reforming catalyst (Hifuel^{TM}) was also studied in the same conditions. A recycling experiment was also performed to evaluate the catalytic activity after a simple regeneration step.

In the second part, the influence of H_2S on the catalytic performance was evaluated with the 10 wt. % Ni/γ-Al_2O_3 catalyst synthesized by the sol-gel process. Two types of experiments were performed: pulse of 200 ppmv of H_2S, or continuous flow of 40 ppmv of H_2S.

2. Materials and Methods

2.1.Nickel-based catalysts

Samples 10Ni, 10Ni-2Mn-2Mo, 10Ni-1.5Ce-1.5K and 10Ni-1.5Ca-1.5K were chosen for long-term catalytic experiments. These catalysts are identical to those studied in [34,35]. They were synthesized by an aqueous sol-gel method, according to [28,29].

In this work, the catalytic performance of a commercial nickel-based steam reforming catalyst (called Hifuel^{TM} R110), from the Johnson Matthey company, was also investigated for

comparison with our sol-gel samples. This catalyst is mostly used in natural gas, liquefied petroleum gas and methane steam reforming applications [37]. It has occasionally been used for the reforming of toluene [38]. For readability, this sample is called Hifuel in this work.

2.2.Materials characterization

Samples composition was determined by inductively coupled plasma–atomic emission spectroscopy (ICP–AES), equipped with an ICAP 6500 THERMO Scientific device [28]. Solid samples were crushed and then dissolved with lithium tetraborate before analysis. Aluminum and nickel loadings were obtained by comparison with standard solutions in the same medium [28].

Textural properties (as specific surface area, S_{BET}, and porous volume, V_p) were determined thanks to nitrogen adsorption-desorption isotherms, measured at -196 °C on a Micromeretics ASAP 2010 instrument after 12 h of outgassing at 300 °C and 10^{-5} Pa [28]. The microporous volume, V_{DR}, is calculated by the Dubinin-Raduskevitch method on the first branch of the adsorption curves at low relative pressure ($p/p_0 < 0.4$) [28]. The pore size distribution is determined by the Broekhoff de Boer method (BdB) applied to the adsorption curve of the nitrogen isotherm [39].

Mercury porosimetry measurements were performed on crushed samples between 300 and 700 µm using a Poremaster 60 instrument from Quantachrome with pressures from 1 to 60,000 Psi. The measurements allowed to determine the macroporous volume (V_{Hg}, cm^3/g), to plot the curves of the volume injected as a function of the pressure and to plot the macropore size distribution [29,40].

The crystallographic properties of samples were determined by X-Ray diffraction (XRD) on a diffractometer Siemens D5000 (Cu-K_α radiation) between 30° and 80° (2θ) with a step time of 18 s and a step size of 0.04° [28]. The Scherrer equation was used to calculate the

crystallite sizes of: (i) alumina, based on the (4 0 0) ray γ-Al_2O_3 (*i.e.* $2\theta = 67.0^\circ$), (ii) $Ni^{(0)}$, based on the (2 0 0) ray (*i.e.* $2\theta = 51.83°$), (iii) $Mo^{(0)}$, based on the Mo (2 1 1) ray (*i.e.* $2\theta = 73.70°$) and (iv) Ni-M alloys (M = Mn or Mo), based on the Ni-M (2 0 0) ray.

The size of metallic particles and their distribution were measured by transmission electron microscopy (TEM) performed on a CM10-PW6020 Philips Electron Microscope. A mean diameter was estimated on 100 particles on TEM micrographs [28]. First, powdered samples were dispersed in absolute ethanol. Then a drop of the dispersion was placed on a copper grid (Formvar/Carbon 200 Mesh Cu from Agar Scientific) [28].

H_2 reduction steps were performed on 1 g of sample with the same protocol as in [34,35].

Temperature Programmed Reduction measurements were performed with a TPD/R/O 1100 device from CE instruments to determine the reduction state of the metallic species in the samples [28]. An amount of 0.2 g of catalyst was placed in a quartz tube. Samples were heated from 25 °C to 1000 °C with a heating rate of 2 °C/min and under 20 mL/min of a gas mixture (5 vol.% H_2 /95 vol.% N_2) [28].

After the catalytic experiments, carbon deposits were calculated by thermogravimetric (TG) and differential scanning calorimetry (DSC), with a Sensys Setaram instrument. Samples were heated from 25 to 800 °C with a heating rate of 2 °C/min under air (20 mL/min) [28].

2.3.Catalytic experiments

The samples were tested at 650 °C, in a reactor described in [28,41]. The catalytic activities were evaluated thanks to the toluene conversion (C_T), the benzene selectivity (S_B), the methane conversion (C_{CH4}) and the toluene reforming rate (r_T) whose formulae are fully detailed in [41]. C_T, S_B and C_{CH4} average values were calculated from the results of the last 10 measurements of each experiment.

Three types of experiments were performed:

2.3.1. *Long-term experiments*

Long-term catalytic experiments were performed under operating conditions similar to those used in our previous studies [28,41]: a temperature of 650 °C, a standard gas mixture (31.5 %vol. H_2, 31.5 %vol. CO, 15.2 %vol. CO_2, 11 %vol. H_2O, 10 %vol. CH_4) and a toluene concentration of 24,000 ppmv. The mass of catalyst was 300 mg, for a catalytic bed height of 12 mm, with a gas flowrate of 50 mL/min and consequently a Gas Hourly Space Velocity (*GHSV)* of 5000 h^{-1} (residence time of 0.72 s). The tests were performed for 30 h, with a Gas Chromatography (GC) injection every 30 min.

2.3.2. *Recycling experiments*

Some catalysts used in long-term experiments were regenerated under air. Same experiments of 30 h, called recycling experiments, were conducted with those catalysts following the same protocol as in Section 2.3.1. For the regeneration, the used-catalysts were heated in the reactor to 650 °C under air for 2 h. The materials can then be re-used.

2.3.3. *Experiment with pulse feed of H_2S*

The conditions of the experiment (mass of catalyst, gas composition, temperature, and gas flowrate) were similar as during a standard experiment. However, the catalytic experiment was interrupted twice, at 90 min and 195 min, to perform the pulse of H_2S as follows:

(i) bypass of the syngas mixture and purge of the reactor for 5 min with 30 mL/min of He;

(ii) injection of a continuous flow of N_2/H_2S mixture with 30 mL/min (200 ppmv of H_2S) for 5 min;

(iii) purge of the reactor for 5 min with 30 mL/min of He;

(iv) injection of the syngas mixture.

The syngas composition can vary and especially its H_2S content; those experiments simulate this variation of H_2S concentration.

The pulse experiments allowed to study the behavior of the catalyst related to a temporary variation of H_2S content. Typically, could the catalyst be regenerated during the experiment itself (under syngas) once the H_2S feed is switched off? Or did the H_2S poisoning reduce drastically the activity? Was the activity recovered even after several pulses simulating consecutive H_2S contaminations?

2.3.4. Experiment with continuous feed of H_2S

In this case, the gas flowrate was composed of 40 mL/min of standard syngas and 10 mL/min of N_2/H_2S mixture (200 ppmv of H_2S), thus corresponding to a global concentration of 40 ppmv of H_2S. The mass of catalyst was 240 mg, in order to keep a *GHSV* of 5000 h^{-1}, when taking into account exclusively the syngas mixture as the feed gas. The catalytic experiments started without H_2S (injection of syngas mixture + pure N_2). After 90 min, the pure N_2 was replaced by the N_2/H_2S mixture until the end of the experiment.

3. Results and Discussion

3.1.Characterization of the sol-gel catalysts

The characterizations of the 4 sol-gel samples were published in [34,35]. The next paragraphs summarize their physico-chemical properties.

Table 2 shows the composition of all sol-gel catalysts. The theoretical and actual loadings were similar for all samples. The textural properties (S_{BET}, V_p, and V_{DR}) are also presented in Table 2 for all samples. They were micro- and mesoporous; as an example, the isotherms of 10Ni and 10Ni-1.5Ca-1.5K are presented in Figure S1 in the Supplementary Materials. At these

low loadings, the element doping had no visible influence on the textural properties of the samples [34,35]. The pore size distributions were quite similar for the four samples (Figure S2).

The metallic particles sizes were estimated after reduction and after TPR analysis. The values, determined by TEM (d_{TEM}) and XRD (d_{XRD}), are compared in Table 3. TEM pictures of the samples after TPR measurements are presented in Figure 1, darker spots corresponding to the nickel particles.

The TPR profiles are presented in Figure 2 for all sol-gel samples. A simultaneous reduction of the MnO_x and MoO_x species was observed in the reduction profile of 10Ni-2Mn-2Mo at 425 °C and 550 °C respectively (Figure 2) [34,35]. The 10Ni-2Mn-2Mo sample also showed a shift of the reduction step of nickel towards lower temperatures (peak located around 800 °C instead 850 °C for the 10Ni sample) (Figure 2) [34,35]. The analysis of the X-Ray pattern after TPR measurements (Figure S3) suggested the presence of a $Ni_{0.9}Mo_{0.1}$ alloy. The association of Mn and Mo apparently decreased the sintering of the metallic particles since d_{XRD} (21 nm), d_{TEM} (25 nm), and associated standard deviation σ_{TEM} (5 nm), were lower for 10Ni-2Mn-2Mo than for 10Ni (Table 3) [34,35].

The 10Ni-1.5Ca-1.5K sample showed a small and broad peak located between 450 °C and 625 °C (Figure 2). This peak was attributed to the presence of Ca and K, reducing the interactions between Ni and γ-Al_2O_3 [42,43]. The 10Ni-1.5Ca-1.5K sample did not show any shift of the principal Ni reduction peak; it was still located around 850 °C as for the 10Ni sample [34,35].

For the 10Ni-1.5Ce-1.5K sample, a peak of very small intensity was also observed between 400 °C and 600 °C (Figure 2) [34,35]. Furthermore, the main peak of Ni reduction at 850 °C was broadened and shifted towards higher temperatures, highlighting the presence of strong Ni-CeO_x interactions [34,35]. The 10Ni-1.5Ca-1.5K and 10Ni-1.5Ce-1.5K samples presented similar particle sizes (Table 3).

3.2. Characterization of the commercial catalyst

The actual composition of the commercial steam reforming catalyst (Hifuel) is included in Table 2. This catalyst was mainly composed of Al_2O_3, Ni and CaO.

The textural properties obtained by nitrogen adsorption-desorption (S_{BET}, V_p and V_{DR}) and the macroporous volume (V_{Hg}) obtained by mercury porosimetry are presented in Table 2. The nitrogen adsorption-desorption isotherm is presented in Figure 3a.

As observed in Figure 3a, at low p/p_0 values, Hifuel sample presented a very low adsorbed volume. Therefore, the microporous volume of this sample was very low (V_{DR} = 0.008 cm^3/g) (Table 2). Furthermore, this sample had a very low specific surface area (S_{BET} = 20 m^2/g) and a low porous volume at saturation pressure of nitrogen (V_p = 0.08 cm^3/g). At higher pressure ($p/p_0 > 0.8$), sample Hifuel presented a slight hysteresis loop, characteristic of the presence of mesopores [39]. Indeed, the mesopore size distribution (Figure 3b) was wide, varying from 2 to 50 nm. However, the mercury porosimetry measurement pointed out that the sample can be considered as non macroporous (V_{Hg} of only 0.2 cm^3/g, Table 2).

X-Ray diffraction was performed on Hifuel sample as received. Four phases were observed in the X-Ray pattern (not shown here): i) corindon alumina, *i.e.* α-Al_2O_3, responsible for the low micro- and mesoporous texture [4]; ii) grossite, *i.e.* $CaAl_4O_7$, obtained by calcination of CaO and Al_2O_3 at high temperatures (T ~ 1000 °C)[44]; iii) bulk nickel oxide, NiO; iv) spinels of nickel aluminate ($NiAl_2O_4$). After TPR (Figure 4a), the NiO rays disappeared and intense rays of $Ni^{(0)}$ appeared at 2θ = 44.4°, 51.8° and 76.3°. The X-Ray pattern of Hifuel sample presented very similar rays of α-Al_2O_3 and $CaAl_4O_7$ after TPR to those before treatment.

The TPR profile, presented in Figure 4b, evidenced that Hifuel sample contained the three different types of nickel oxides: bulk NiO (reduction at T ~ 450 °C), NiO/Al_2O_3 (reduction at T ~ 625 °C) and $NiAl_2O_4$ (reduction at T ~ 775 °C) [45,46]. The Ni particles size was determined after reduction and after TPR by TEM and XRD. The values are presented in Table 3. After H_2

reduction, Hifuel sample was composed of large Ni particles (d_{TEM} = 26 nm and d_{XRD}= 23 nm) with a broad distribution of size (σ_{TEM} = 15 nm). After TPR, the Ni particles in Hifuel sample became larger (d_{TEM} = 32 nm and d_{XRD}= 34 nm), with a very high σ_{TEM} value (26 nm). Large particles and sensitivity to sintering observed for Hifuel sample were caused by two simultaneous factors: i) a low microporous texture, unable to prevent the migration of the metallic particles; ii) a high amount of bulk NiO, known to easily sinter because of its low interactions with the alumina support [45,46].

3.3.Long-term experiments

Figure 5a shows the toluene conversion, C_T, as a function of time for 10Ni, 10Ni-2Mn-2Mo, 10Ni-1.5Ca-1.5K, 10Ni-1.5Ce-1.5K and Hifuel. Figure 5b shows the DSC measurements performed on the samples after the catalytic experiments. The metallic particles sizes, the metallic phases present after the experiments and the catalytic performances of the samples are summarized in Table 4.

After 300 min, the 10Ni sample underwent a progressive deactivation (ΔC_T = - 20 %) (Figure 5a and Table 4). However, for similar operating conditions, the properties of the catalyst remained mainly unchanged after 30 h of reaction in comparison to the 5 h catalytic experiment [34,35]. Indeed, after a long-term experiment, 10Ni sample showed small $Ni^{(0)}$ particles (d_{TEM} and d_{XRD} = 12 nm) with a narrow distribution of size (σ_{TEM} = 4 nm), and the amount of carbon deposit was only doubled (after 30 h: *Coke* = 0.20 g_{Carbon}/g_{Cata}; whereas after 5 h: *Coke* = 0.10 g_{Carbon}/g_{Cata} [34,35]). Furthermore, Figure 5b evidenced that the carbon deposit on 10Ni sample was mostly composed of amorphous carbon (burned at T < 550 °C), no carbon nanotube was detected by TEM (Figure S4a). This was also observed after the 5 h catalytic experiment. The X-Ray pattern (Figure S5) obtained after a long-term experiment did not show any alteration of the γ-Al_2O_3 phase. These observations were very positive. Indeed, since the crystallinity and

the metallic dispersion remained unchanged, and 10Ni sample only presented amorphous carbon after 30 h of reaction, a regeneration step (by injection of air or H_2O) could be considered in order to reactivate the catalyst.

In the case of 10Ni-2Mn-2Mo, 10Ni-1.5Ca-1.5K and 10Ni-1.5Ce-1.5K, the co-doping of 10 wt. % Ni/γ-Al_2O_3 catalysts effectively reduced the loss of catalytic activity (ΔC_T < - 9 %, whereas ΔC_T = - 20 % for the 10Ni sample). Furthermore, all samples presented low amounts of carbon deposits (*Coke* = 0.19 g_{Carbon}/g_{Cata} for 10Ni-2Mn-2Mo and 10Ni-1.5Ca-1.5K, and *Coke* = 0.28 g_{Carbon}/g_{Cata} for 10Ni-1.5Ce-1.5K) and relatively low $Ni^{(0)}$ particles sizes (Table 4) were maintained. Since these samples are mostly covered by amorphous carbon, they are also good candidates for further industrial applications. They could be reused after a regeneration in soft conditions.

In Figure 5a, Hifuel sample showed a very high initial C_T, followed by a quick and intense deactivation (ΔC_T = - 50 % after 300 min). The formation of coke for this sample was so important that it increased the pressure drop inside the reactor and forced to stop the experiment at 300 min. DSC (Figure 5b) and TEM measurements (Figure 1f and S4b) performed after the catalytic experiment highlighted that nearly the entire carbon deposit was filamentous. These results have to be correlated with the ones obtained for the Ni/γ-Al_2O_3 catalysts studied in [28,29]. Hence, the strong deactivation observed for Hifuel sample was attributed to a combination of detrimental factors. First, Hifuel sample contained large amounts of bulk NiO. This type of nickel oxide was reduced at a temperature of 450 °C lower than the operating temperature (650 °C), making the mechanism of "special reduction by toluene" and its anti-coking effect inapplicable [28]. Furthermore, because of its high catalytic activity and its low interactions with the support, NiO was quickly deactivated. Its low interactions with the support also make it more sensitive to sintering. This leads to the formation of large $Ni^{(0)}$ particles, accentuating the formation of filamentous carbon. This last effect was assumed to be reinforced

by the very low micro- and mesoporous texture of Hifuel sample (Table 2). Though the high amount of CaO might increase the rate of adsorption-dissociation of H_2O and CO_2 molecules, the very low specific surface area of Hifuel sample (S_{BET} = 20 m^2/g, Table 2) reduced the surface available for these reactions to take place. Finally, the presence of large mesopores (Figure 3) was assumed to favor the formation of coke: i) by an increased diffusion of the reactants through the catalyst reinforcing the disequilibrium between the reaction rates of toluene cracking and those of gasification; and ii) by the difficulty for very large pores to prevent the formation of filamentous carbon [29].

Therefore, despite the interesting performances of the Hifuel catalyst for the steam reforming of various compounds (glycerol, ethanol, methane …) [37], including toluene (noteworthy in less intense conditions: only 5,000 ppmv of toluene and a high H_2O/C ratio equal to 2) [38], this catalyst must be proscribed for tar reforming applications. The concentration of toluene was much higher in our study than in common conditions (usually, tar concentration between 1,000-10,000 ppmv). However it is assumed that, if Hifuel sample is not resistant against deactivation by coking in presence of toluene, it would probably be also deactivated in presence of high deactivating tars such as naphthalene or pyrene.

3.4.Long-term experiments after regeneration

The activity of 10Ni, 10Ni-2Mn-2Mo and 10Ni-1.5Ca-1.5K catalysts was evaluated after regeneration under air. The toluene conversion is presented in Figure 6 as a function of time over the 30 h of experiment. The deactivation was lower for the two co-doped samples than for the 10Ni sample; their activity remained nearly constant during the 30 h. The deactivation of 10Ni sample is stronger but followed a curve similar to the one before regeneration (Figure 5a) with a toluene conversion value around 31 % after 30 h. The conversion reached 53% both for 10Ni-2Mn-2Mo and 10Ni-1.5Ca-1.5K samples (Figure 5a – Table 4). The toluene conversion

was also similar before and after regeneration, for both samples. With the two successive experiments, the activity of catalysts was henceforth maintained up to 60 h of operation. The catalytic activity was therefore not affected by the regeneration, a clear advantage for industrial applications.

Moreover, the morphology of 10Ni sample was not modified by the regeneration. The nitrogen adsorption-desorption isotherm (Figure S6) and the XRD pattern (Figure S7) after regeneration were similar to the initial ones (Figure S1 and S5). Therefore, the texture and the crystallinity of 10Ni sample stayed similar before catalytic experiment and after regeneration.

A direct comparison with the literature is difficult due to the various operating conditions, as the concentration of toluene, the temperature of reaction or the duration of the catalytic experiment. In Heo *et al.* [47], Ni-based catalysts impregnated on α-Al_2O_3, olivine or dolomite were doped with Mn, Ca or K in order to produce carbon resistant catalysts for toluene reforming. The toluene reforming was performed at 800 °C during 5 h with a toluene concentration of 1,000 ppmv. In this study, no regeneration or long-term experiments were performed, and a conversion around 60 % was obtained. In Iida *et al.* [48], Ru/$SrCO_3$-Al_2O_3 catalysts were used for toluene (~52,000 ppm) reforming at 600 °C. The conversion reached 50 % after 180 min with the best catalyst. The catalytic activity was measured only during 3 h and no regeneration of the catalyst was performed. In Quan *et al.* [49], Ni supported on biochar was used as toluene reforming (416 ppm) catalyst. Cerium was added to improve the catalyst stability. With the best catalyst, 80 % of toluene was converted after 160 min at 600 °C. In this study, a stability experiment was performed during 18 h, only the H_2 production was reported during this experiment. The Ce addition limited the decrease of H_2 production around 25 % after the 18 h. No regeneration was performed. In Xu *et al.* [50], carbon-coated mesoporous silica-supported Ni nanocomposite catalyst was used for the production of H_2 from toluene reforming. Long-term stability study was performed on toluene reforming (4,000 ppm) for 46

h at 550 °C with a complete conversion of toluene. This very high conversion was due to (i) high interactions between Ni nanoparticles and the support, and (ii) a specific morphology of the catalyst with the carbon coated Ni nanoparticles avoiding the sintering of the metal active phase. In Li *et al*. [31], Ni–Fe/Mg/Al catalysts were synthesized by co-precipitation followed by calcination/reduction. These catalysts were used for tar reforming from real biomass (cedar wood). The regeneration of the catalysts was investigated; a treatment at 873 K under oxidative atmosphere was applied for 1 h. The stability of the activity was assessed during three cycles of regeneration, corresponding to a 1 h catalytic experiment followed by a 1 h regeneration. The results showed that the activity was recovered after each regeneration step, removing the carbon deposit. The interactions between the Ni–Fe alloy nanoparticles and the MgO-based mixed oxides played a crucial role in the enhanced regenerability [31].

3.5.Catalytic performances of 10Ni sample in sulphidic conditions

Figure 7 presents the toluene conversion in sulphidic environments for the two types of experiments: (i) a standard reforming experiment interrupted with pulses of 200 ppmv of H_2S (10Ni-Pulse) or (ii) a standard catalytic experiment with a continuous flow of 40 ppmv of H_2S (10Ni-Continuous). The evolution of the catalytic performances during the experiments are presented in Table 5 as well as the sizes of the metallic nickel particles determined by XRD and TEM after the catalytic experiments. Figure 8 shows the DSC curves obtained after the catalytic experiments.

X-Ray measurements were performed after both catalytic experiments (Figure S5). For both tests, the spectra only presented rays of γ-Al_2O_3 and $Ni^{(0)}$, and no nickel sulfide rays (such as Ni-S or Ni_3S_2) were observed. It was assumed that (i) none of these species were present, because of regeneration reactions (Reactions (3) and (4) in Table 1), or (ii) these species covered

only the $Ni^{(0)}$ particles, and hence were in insufficient amounts to be detected by X-Ray diffraction.

Regarding the 10Ni-Pulse experiment (Figure 7a), after the first pulse of H_2S, the conversion of toluene was considerably increased (ΔC_T = + 15 %). This observation suggests that the injection of a mixture of H_2S (200 ppmv)/He increased the reduction of the catalyst via the Reaction (1) (Table 1). Once the syngas was reinjected, the NiS species were regenerated by the H_2 and H_2O compounds via Reactions (3) and (4). This assumption is based on the fact that 10Ni-Pulse sample presented a high C_{CH4} value at the end of the experiment (10 %, Table 5), and that the conversion of methane is usually more affected by sulphide deactivation than the conversion of tars [51]. Furthermore, the higher C_T value and the lower S_B value for 10Ni-Pulse sample suggested that a higher amount of nickel was catalytically active.

10Ni-Pulse sample presented similar d_{TEM} and d_{XRD} values to the ones obtained during a standard catalytic experiment without H_2S (Tables 4 and 5). This observation is interesting, since Ni-S compounds are more sensitive to sintering than pure $Ni^{(0)}$ [21]. However, the metallic particles size distribution (σ_{TEM} = 6 nm) of 10Ni-Pulse sample was broader than the one observed during a standard experiment (σ_{TEM} = 3 nm for 10Ni sample [28]). The presence of some larger $Ni^{(0)}$ particles, highlighted by the higher σ_{TEM} value, could explain why a small part of filamentous carbon was observed in the DSC curve of 10Ni-Pulse sample (Figure 8).

Regarding the 10Ni-Continuous sample (Figure 7b), the addition of 40 ppmv of H_2S led to a slight increase of the C_T value during the first 45 min of reaction. Here also, it was assumed that the addition of H_2S increased the reduction of Ni. However, from 135 min to the end of the experiment, the C_T value slightly decreased (ΔC_T = - 11 %). This influence was more obvious for the methane conversion since the C_{CH4} value dropped to 1 % at the end of the experiment (Table 5). These observations suggested a partial deactivation of the surface of the $Ni^{(0)}$ particles by the formation of Ni-S compounds [21]. Furthermore, though d_{TEM} and d_{XRD} values remained

small, 10Ni-Continuous sample showed a broad distribution of metallic particles size (σ_{TEM} = 8 nm, Table 5). The presence of larger particles led to a higher formation of filamentous carbon, as highlighted in the DSC curve (Figure 8). In that case, the sensitivity of the sample to sintering was attributed to the formation of Ni-S compounds, whose Tamman's temperatures are lower than pure $Ni^{(0)}$ ones [21]. Nevertheless, the sulfur contamination was relatively low as no peak associated to NiS or other sulfur compound was observed on the XRD pattern (Figure S5).

Therefore, instead of protecting the $Ni^{(0)}$ particles from coking by "ensemble control" effect [4], the presence of H_2S favored the formation of filamentous carbon.

Finally, the loss of catalytic activity for the reforming of toluene was relatively small for 10Ni-Continuous sample compared to literature for this amount of H_2S and at this temperature [4]. The following assumptions could explain the very good resistance against deactivation by H_2S: (i) the Ni particles have strong interactions with the γ-Al_2O_3 support ($NiAl_2O_4$ evidenced by TPR in [28]); it would facilitate the migration of the O^* and HO^* species from the support to the $Ni^{(0)}$ particles and increase the regeneration reaction of the deactivated sites Ni-S (Reactions (3) and (4)); (ii) this effect could be emphasized since the catalyst was tested at the boundary conditions between the oxidation and the reduction of Ni.

Specific study on H_2S resistance of Ni catalysts for toluene reforming in similar conditions was not found in literature. The following paragraph reviewed some studies about catalysts for tar reforming and H_2S resistance. In Dou *et al.* [24], the poisoning effect of H_2S (continuous feed - 50 ppmv) on Ni catalysts was evaluated on the reforming of naphthalene. At 850 °C, the naphthalene conversion decreased by about 5 % after 300 min of experiment due to the H_2S poisoning. In Quitete *et al.* [25], Ni/perovskite catalysts were used for toluene reforming under H_2S (50 ppmv - continuous feed) at 800 °C. After 3 h of reaction, the conversion decreased by 15 % in the presence of H_2S and after 26 h, the conversion fell to 50%. This high decrease was due to nickel sulfide formation and very high coke deposition. In Ashok *et al.* [26],

Ce_2O/perovskite materials were used for toluene reforming. The impact of H_2S was studied; 50 ppm of H_2S was injected in pulse during toluene reforming at 750 °C leading to deactivation. Then a partial recovery of the activity was obtained due to the regeneration of the active site during the experiment. In Tomishige *et al.* [33], $Rh/CeO_2/SiO_2$ catalysts were studied on the tar reforming of biosyngas produced from cedar wood. A commercial Ni-based catalyst was also tested. The concentration of H_2S was 280 ppm and the temperature 823 K. The stability of the catalytic activity was greater for the $Rh/CeO_2/SiO_2$ catalysts than for the commercial one due to the low affinity of sulfur for their catalyst. Indeed, almost no sulfur was detected at the catalyst surface [33].

4. Conclusions

In this work, the catalytic performances of promising sol-gel Ni/γ-Al_2O_3 catalysts were studied in severe conditions (long-term experiments or in presence of H_2S). Those catalysts were identified throughout previous studies. Their performances were compared with a commercial nickel-based steam reforming catalyst for the reforming of 24,000 ppmv of toluene: commercial Hifuel^{TM} catalyst.

The sol-gel 10 wt. % Ni/γ-Al_2O_3 catalyst presented a low but progressive deactivation throughout the 30 h of experiment. However, this sample maintained very small $Ni^{(0)}$ particles with a narrow size distribution, without any alteration of the crystallinity of the γ-Al_2O_3 support and it only presented amorphous carbon. These observations were positive since they opened the way for catalytic experiments with easy regeneration step. After regeneration under air, the catalyst recovered a similar conversion as before recycling.

All 10 wt. % Ni/γ-Al_2O_3 catalysts co-doped with Mn+Mo, Ca+K or Ce+K showed a better resistance against deactivation than pure 10 wt. % Ni/γ-Al_2O_3 catalyst. Furthermore, as their interesting properties remained unchanged after 30 h of catalytic experiments, a simple and

non-destructive regeneration under air was carried out. The activity of the catalysts remained constant with a conversion similar to the one obtained after the first 30 h of experiment.

The strong and quick deactivation observed for commercial Hifuel^{TM} catalyst confirmed the importance of designing catalysts with metal/support interactions adapted to the conditions of experiment, in order to take advantage of the anti-coking effect brought by the "mechanism of special reduction by toluene".

The 10 wt. % Ni/γ-Al_2O_3 catalyst was only slightly affected by the presence of H_2S in the syngas mixture. This was attributed to two factors: (i) the Ni particles have strong interactions with the γ-Al_2O_3 support; it would facilitate the migration of the O^* and HO^* species from the support to the $Ni^{(0)}$ particles, and favor the regeneration reactions of the deactivated sites Ni-S; (ii) this effect could be accentuated by the operating conditions at the boundary between the oxidation and the reduction of Ni.

Author Contributions:

Conceptualization and methodology, V.C., T.L., F.M. and S.D.L.; investigation, analysis and writing, V.C., J.G.M., S.D., T.L., F.M. and S.D.L., writing-original draft preparation, J.G.M., S.D. and S.D.L.; supervision, funding acquisition and project administration, S.D.L. All the authors corrected the paper before submission and during the revision process.

Compliance with ethical standards

Conflict of interest: The authors declare that they have no conflicts of interest.

Data availability

The raw/processed data required to reproduce these findings cannot be shared at this time as the data also forms part of an ongoing study.

Acknowledgements

V. C. thanks the F.R.S.-F.N.R.S. for his doctoral grant obtained with the "Fonds de Recherche collective" n° 2.4541.12. S. D. L. is also grateful to F.R.S.-F.N.R.S for her Senior Research

Associate position. The authors also acknowledge the Ministère de la Région Wallonne Direction Générale des Technologies, de la Recherche et de l'Energie (DGO6) and the Fond de Bay for financial supports.

References

[1] M.A. Goula, N.D. Charisiou, K.N. Papageridis, A. Delimitis, E. Pachatouridou, E.F. Iliopoulou, Nickel on alumina catalysts for the production of hydrogen rich mixtures via the biogas dry reforming reaction: Influence of the synthesis method, Int. J. Hydrogen Energy. 40 (2015) 9183–9200. doi:10.1016/j.ijhydene.2015.05.129.

[2] G. Guan, M. Kaewpanha, X. Hao, A. Abudula, Catalytic steam reforming of biomass tar: Prospects and challenges, Renew. Sustain. Energy Rev. 58 (2016) 450–461. doi:10.1016/j.rser.2015.12.316.

[3] Z. Zhang, L. Liu, B. Shen, C. Wu, Preparation, modification and development of Ni-based catalysts for catalytic reforming of tar produced from biomass gasification, Renew. Sustain. Energy Rev. 94 (2018) 1086–1109. doi:10.1016/j.rser.2018.07.010.

[4] V. Claude, C. Courson, M. Köhler, S.D. Lambert, Overview and Essentials of Biomass Gasification Technologies and Their Catalytic Cleaning Methods, Energy and Fuels. 30 (2016) 8791–8814. doi:10.1021/acs.energyfuels.6b01642.

[5] V. Claude, C. Courson, M. Köhler, S.D. Lambert, Correction to overview and essentials of biomass gasification technologies and their catalytic cleaning methods (Energy Fuels (2016) 30:11 (8791-8814) DOI: 10.1021/acs.energyfuels.6b01642), Energy and Fuels. 31 (2017) 1050. doi:10.1021/acs.energyfuels.6b03436.

[6] D. Li, Y. Nakagawa, K. Tomishige, Development of Ni-Based Catalysts for Steam Reforming of Tar Derived from Biomass Pyrolysis, Chinese J. Catal. 33 (2012) 583–

594. doi:10.1016/S1872-2067(11)60359-8.

[7] F.L. Chan, A. Tanksale, Review of recent developments in Ni-based catalysts for biomass gasification, Renew. Sustain. Energy Rev. 38 (2014) 428–438. doi:10.1016/j.rser.2014.06.011.

[8] D. Świerczyński, S. Libs, C. Courson, a. Kiennemann, Steam reforming of tar from a biomass gasification process over Ni/olivine catalyst using toluene as a model compound, Appl. Catal. B Environ. 74 (2007) 211–222. doi:10.1016/j.apcatb.2007.01.017.

[9] J.N. Kuhn, Z. Zhao, A. Senefeld-Naber, L.G. Felix, R.B. Slimane, C.W. Choi, et al., Ni-olivine catalysts prepared by thermal impregnation: Structure, steam reforming activity, and stability, Appl. Catal. A Gen. 341 (2008) 43–49. doi:10.1016/j.apcata.2007.12.037.

[10] Z. Zhao, N. Lakshminarayanan, J.N. Kuhn, A. Senefeld-Naber, L.G. Felix, R.B. Slimane, et al., Optimization of thermally impregnated Ni–olivine catalysts for tar removal, Appl. Catal. A Gen. 363 (2009) 64–72. doi:10.1016/j.apcata.2009.04.042.

[11] M.M. Yung, W.S. Jablonski, K. a. Magrini-Bair, Review of Catalytic Conditioning of Biomass-Derived Syngas, Energy & Fuels. 23 (2009) 1874–1887.

[12] S. Anis, Z. a. Zainal, Tar reduction in biomass producer gas via mechanical, catalytic and thermal methods: A review, Renew. Sustain. Energy Rev. 15 (2011) 2355–2377. doi:10.1016/j.rser.2011.02.018.

[13] L. Cao, I.K.M. Yu, X. Xiong, D.C.W. Tsang, S. Zhang, J.H. Clark, et al., Biorenewable hydrogen production through biomass gasification: A review and future prospects, Environ. Res. 186 (2020) 109547. doi:10.1016/j.envres.2020.109547.

[14] J. Ashok, N. Dewangan, S. Das, P. Hongmanorom, M. Hui, K. Tomishige, et al.,

Recent progress in the development of catalysts for steam reforming of biomass tar model reaction, Fuel Process. Technol. 199 (2020) 106252. doi:10.1016/j.fuproc.2019.106252.

[15] D. Dayton, A review of the literature on catalytic biomass tar destruction, Natl. Renew. Energy Lab. (2002) 28.

[16] A.M. Dăncilă, S. Căprărescu, C. Bobirică, V. Purcar, G. Gârleanu, E. Vasile, et al., Optimization of the technological parameters for obtaining Zn-Ti Based Composites to increase the performance of H2S removal from syngas, Processes. 8 (2020). doi:10.3390/PR8050562.

[17] I.A. Mkhalid, A. Shawky, Visible light-active CdSe/rGO heterojunction photocatalyst for improved oxidative desulfurization of thiophene, Ceram. Int. (2020) 0–1. doi:10.1016/j.ceramint.2020.05.033.

[18] A. Shawky, R.M. Mohamed, I.A. Mkhalid, N.S. Awwad, H.A. Ibrahium, One-pot synthesis of Mn3O4-coupled Ag2WO4 nanocomposite photocatalyst for enhanced photooxidative desulfurization of thiophene under visible light irradiation, Appl. Nanosci. 10 (2020) 1545–1554. doi:10.1007/s13204-019-01212-0.

[19] A. Shawky, M. Alhaddad, K.S. Al-Namshah, R.M. Mohamed, N.S. Awwad, Synthesis of Pt-decorated CaTiO3 nanocrystals for efficient photoconversion of nitrobenzene to aniline under visible light, J. Mol. Liq. 304 (2020) 112704. doi:10.1016/j.molliq.2020.112704.

[20] M. Alhaddad, A. Shawky, Superior photooxidative desulfurization of thiophene by reduced graphene oxide-supported MoS2 nanoflakes under visible light, Fuel Process. Technol. 205 (2020) 106453. doi:10.1016/j.fuproc.2020.106453.

[21] X. Gao, Z. Wang, J. Ashok, S. Kawi, A comprehensive review of anti-coking, anti-

poisoning and anti-sintering catalysts for biomass tar reforming reaction, Chem. Eng. Sci. X. 7 (2020) 100065. doi:10.1016/j.cesx.2020.100065.

[22] C. Xie, Y. Chen, Y. Li, X. Wang, C. Song, Sulfur poisoning of CeO2-Al2O3-supported mono- and bi-metallic Ni and Rh catalysts in steam reforming of liquid hydrocarbons at low and high temperatures, Appl. Catal. A Gen. 390 (2010) 210–218. doi:10.1016/j.apcata.2010.10.012.

[23] J. Gallego, C. Batiot-Dupeyrat, J. Barrault, F. Mondragón, Severe Deactivation of a LaNiO 3 Perovskite-Type Catalyst Precursor with H 2 S during Methane Dry Reforming, Energy & Fuels. 23 (2009) 4883–4886. doi:10.1021/ef900409x.

[24] X. Dou, A. Veksha, W.P. Chan, W. Da Oh, Y.N. Liang, F. Teoh, et al., Poisoning effects of H2S and HCl on the naphthalene steam reforming and water-gas shift activities of Ni and Fe catalysts, Fuel. 241 (2019) 1008–1018. doi:10.1016/j.fuel.2018.12.119.

[25] C.P.B. Quitete, R.L. Manfro, M.M.V.M. Souza, Perovskite-based catalysts for tar removal by steam reforming: Effect of the presence of hydrogen sulfide, Int. J. Hydrogen Energy. 42 (2017) 9873–9880. doi:10.1016/j.ijhydene.2017.02.187.

[26] J. Ashok, S. Das, N. Dewangan, S. Kawi, H2S and NOx tolerance capability of CeO2 doped La1−x CexCo0.5Ti0.5O3−Δ perovskites for steam reforming of biomass tar model reaction, Energy Convers. Manag. X. 1 (2019) 100003. doi:10.1016/j.ecmx.2019.100003.

[27] A. Bassani, C. Pirola, E. Maggio, A. Pettinau, C. Frau, G. Bozzano, et al., Acid Gas to Syngas (AG2S^{TM}) technology applied to solid fuel gasification: Cutting H2S and CO2 emissions by improving syngas production, Appl. Energy. 184 (2016) 1284–1291. doi:10.1016/j.apenergy.2016.06.040.

[28] V. Claude, J.G. Mahy, J. Geens, S.D. Lambert, Ni-doped γ-Al2O3 as secondary catalyst for bio-syngas purification: influence of Ni loading, catalyst preparation, and gas composition on catalytic activity, Mater. Today Chem. 13 (2019) 98–109. doi:10.1016/j.mtchem.2019.05.002.

[29] V. Claude, J.G. Mahy, F. Micheli, J. Geens, S.D. Lambert, Sol-gel Ni/γ-Al2O3 material as secondary catalyst for toluene reforming: Tailoring the γ-Al2O3 substrate with stearic acid, Microporous Mesoporous Mater. 291 (2020) 109681. doi:10.1016/j.micromeso.2019.109681.

[30] F. Cheng, V. Dupont, M. V Twigg, Temperature-programmed reduction of nickel steam reforming catalyst with glucose, Appl. Catal. A Gen. 527 (2016) 1–8. doi:10.1016/j.apcata.2016.08.013.

[31] D. Li, M. Koike, L. Wang, Y. Nakagawa, Y. Xu, K. Tomishige, Regenerability of Hydrotalcite-Derived Nickel – Iron Alloy Nanoparticles for Syngas Production from Biomass Tar, ChemSusChem. 7 (2014) 510–522. doi:10.1002/cssc.201300855.

[32] M. Koike, C. Ishikawa, D. Li, L. Wang, Y. Nakagawa, K. Tomishige, Catalytic performance of manganese-promoted nickel catalysts for the steam reforming of tar from biomass pyrolysis to synthesis gas, Fuel. 103 (2013) 122–129. doi:10.1016/j.fuel.2011.04.009.

[33] K. Tomishige, T. Miyazawa, T. Kimura, K. Kunimori, N. Koizumi, M. Yamada, Resistance to sulfur poisoning of hot gas cleaning catalysts for the removal of tar from the pyrolysis of cedar wood, Appl. Catal. B Environ. 60 (2005) 299–307. doi:10.1016/j.apcatb.2005.04.003.

[34] V. Claude, J.G. Mahy, R.G. Tilkin, S.D. Lambert, Enhancement of the catalytic performances and lifetime of Ni/<gamma>-Al2O3 catalysts for the steam toluene

reforming via the combination of dopants: Inspection of Cu, Co, Fe, Mn and Mo species addition, Mater. Today Chem. 15 (2020) 100229.

[35] V. Claude, J.G. Mahy, T. Lohay, R.G. Tilkin, F. Micheli, S.D. Lambert, Sol – gel synthesis of Ni/Al2O3 catalysts for toluene reforming : Support modification with alkali , alkaline earth or rare-earth dopant (Ca,K,Mg or Ce), Surfaces and Interfaces. 20 (2020) 100511. doi:10.1016/j.surfin.2020.100511.

[36] V. Claude, J.G. Mahy, S. Douven, S.L. Pirard, C. Courson, S.D. Lambert, Ni- and Fe-doped g-Al2O3 or olivine as primary catalyst for toluene reforming, Mater. Today Chem. 14 (2019) 100197. doi:10.1016/j.mtchem.2019.100197.

[37] M.T. Azizan, Steam Reforming of Oxygenated Hydrocarbons for Hydrogen Production, PhD, Imperial College London, 2014.

[38] L.S. Marin, Treatment of biomass-derived synthesis gas using commercial steam reforming catalysts and biochar, PhD Thesis, Oklahoma State University, 2011.

[39] A.J. Lecloux, Texture of catalysts, Catal. Sci. Technol. 2 (1981) 171.

[40] S. Lambert, C. Alié, J.P. Pirard, B. Heinrichs, Study of textural properties and nucleation phenomenon in Pd/SiO2, Ag/SiO2and Cu/SiO2cogelled xerogel catalysts, J. Non. Cryst. Solids. 342 (2004) 70–81. doi:10.1016/j.jnoncrysol.2004.06.005.

[41] V. Claude, J.G. Mahy, J. Geens, C. Courson, S.D. Lambert, Synthesis of Ni/γ-Al2O3-SiO2 catalysts with different silicon precursors for the steam toluene reforming, Microporous Mesoporous Mater. 284 (2019) 304–315. doi:10.1016/j.micromeso.2019.04.027.

[42] K.F.M. Elias, A.F. Lucrédio, E.M. Assaf, Effect of CaO addition on acid properties of Ni–Ca/Al2O3 catalysts applied to ethanol steam reforming, Int. J. Hydrogen Energy. 38 (2013) 4407–4417. doi:10.1016/j.ijhydene.2013.01.162.

[43] X. Hu, G. Lu, Inhibition of methane formation in steam reforming reactions through modification of Ni catalyst and the reactants, Green Chem. 11 (2009) 724–732. doi:10.1039/b814009j.

[44] M. Puchalska, E. Zych, M. Sobczyk, A. Watras, P. Deren, Effect of charge compensation on up-conversion and UV excited luminescence of Eu3+ in Yb3+-Eu3+ doped calcium aluminate CaAl4O7, Mater. Chem. Phys. 147 (2014) 304–310. doi:10.1016/j.matchemphys.2014.05.003.

[45] M. Zangouei, A.Z. Moghaddam, M. Arasteh, The influence of nickel loading on reducibility of NiO/Al2O3 catalysts synthesized by sol-gel method, Chem. Eng. Res. Bull. 14 (2010) 97–102. doi:10.3329/cerb.v14i2.5052.

[46] A.L. Alberton, M.M.V.M. Souza, M. Schmal, Carbon formation and its influence on ethanol steam reforming over Ni/Al2O3 catalysts, Catal. Today. 123 (2007) 257–264. doi:10.1016/j.cattod.2007.01.062.

[47] D.H. Heo, R. Lee, J.H. Hwang, J.M. Sohn, The effect of addition of Ca, K and Mn over Ni-based catalyst on steam reforming of toluene as model tar compound, Catal. Today. 265 (2016) 95–102. doi:10.1016/j.cattod.2015.09.057.

[48] H. Iida, S. Deguchi, M. Torigai, Y. Osawa, Steam reforming of toluene over Ru/SrCO3-Al2O3 catalyst under extremely low steam-to-carbon ratio conditions, Fuel. 272 (2020) 117703. doi:10.1016/j.fuel.2020.117703.

[49] C. Quan, H. Wang, N. Gao, Development of activated biochar supported Ni catalyst for enhancing toluene steam reforming, Int. J. Energy Res. 44 (2020) 5749–5764. doi:10.1002/er.5335.

[50] H. Xu, Z. Shen, G. Chen, C. Yin, Y. Liu, Z. Ge, et al., Carbon-coated mesoporous silica-supported Ni nanocomposite catalyst for efficient hydrogen production via steam

reforming of toluene, Fuel. 275 (2020) 1–8. doi:10.1016/j.fuel.2020.118036.

[51] J. Rostrup-Nielsen, Catalytic Steam Reforming, Catal. Sci. Technol. 5 (1984) 1–117. doi:doi.org/10.1007/978-3-642-93247-2_1.

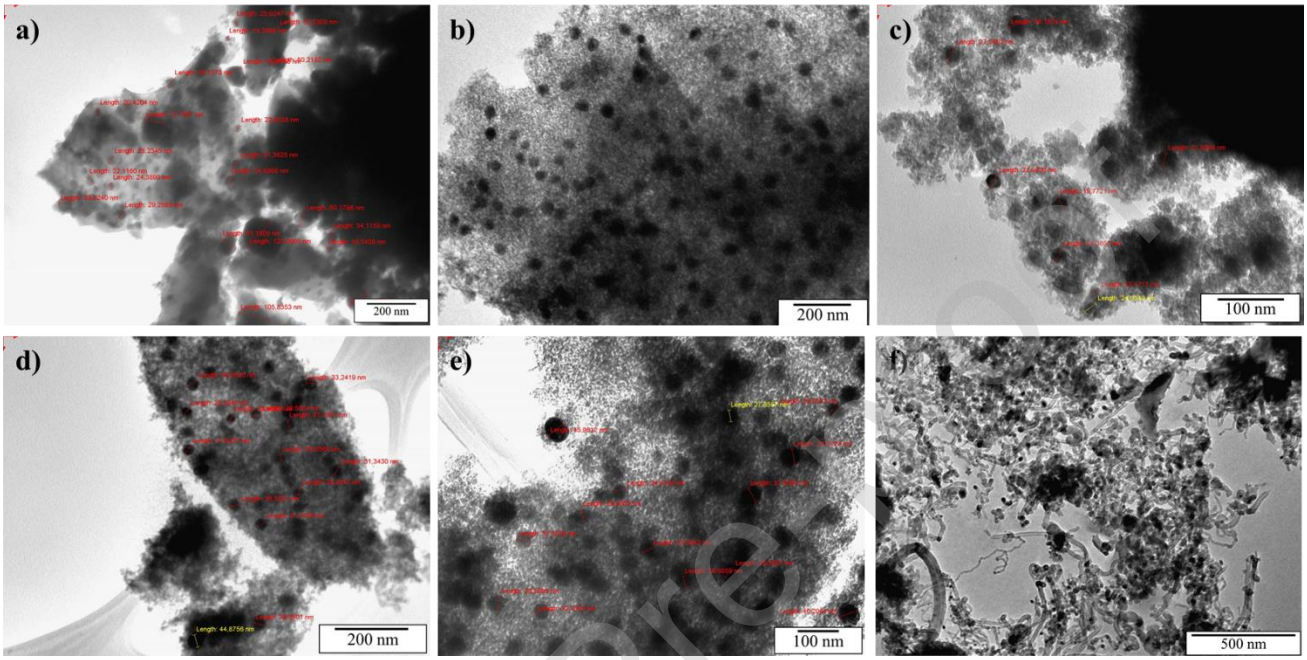

Figure 1: TEM micrographs of (a) Hifuel, (b) 10Ni, (c) 10Ni-2Mn-2Mo, (d) 10Ni-1.5Ca-1.5K, and (e) 10Ni-1.5Ce-1.5K samples after TPR measurements; and (f) Hifuel sample after catalytic experiment.

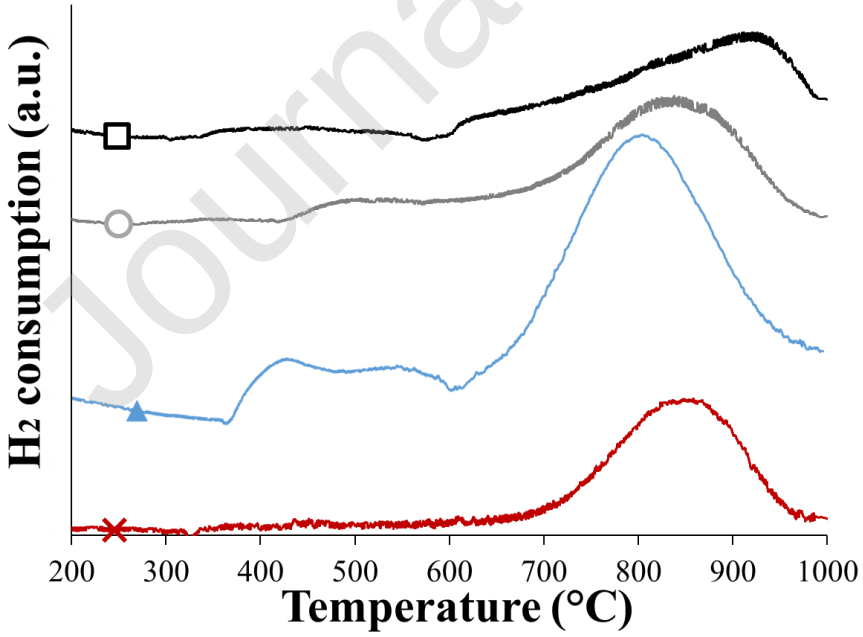

Figure 2: TPR profiles for (×) 10Ni, (▲) 10Ni-2Mn-2Mo, (○) 10Ni-1.5Ca-1.5K, and (□) 10Ni-1.5Ce-1.5K.

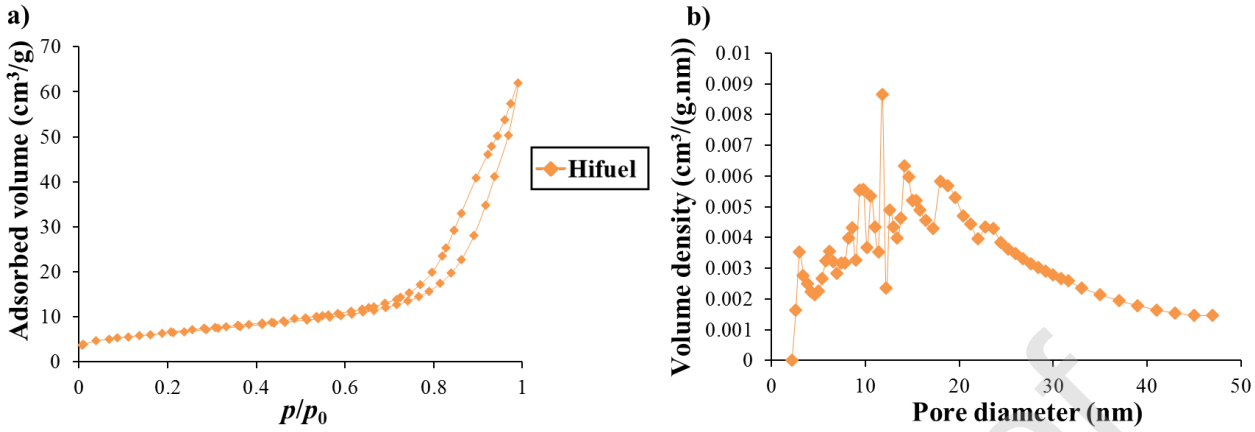

Figure 3: (a) Nitrogen adsorption-desorption isotherm and (b) mesopore size distribution of Hifuel.

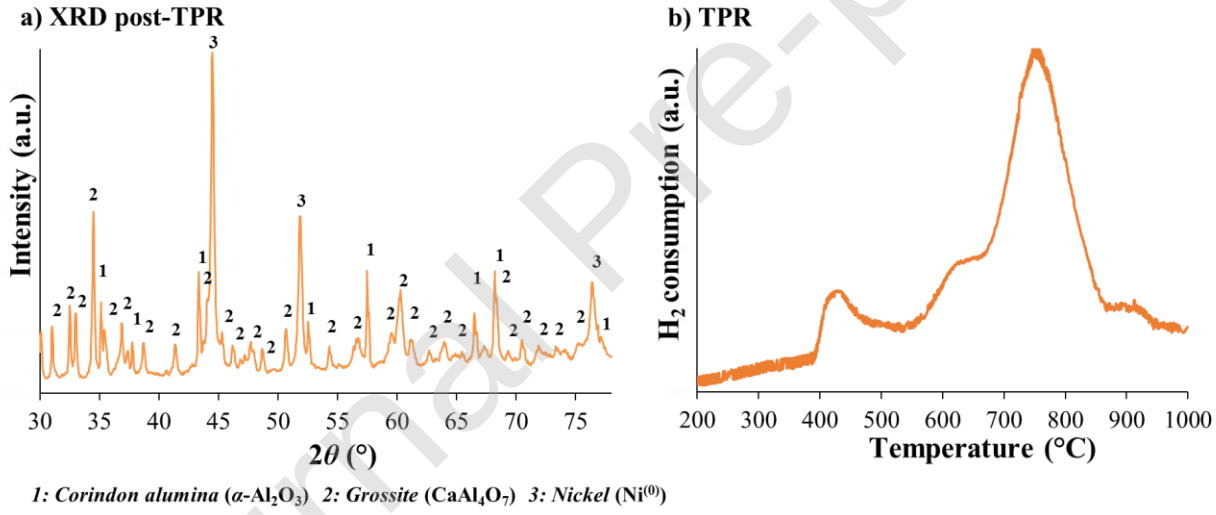

Figure 4: (a) post-TPR XRD pattern and (b) TPR profile of Hifuel sample.

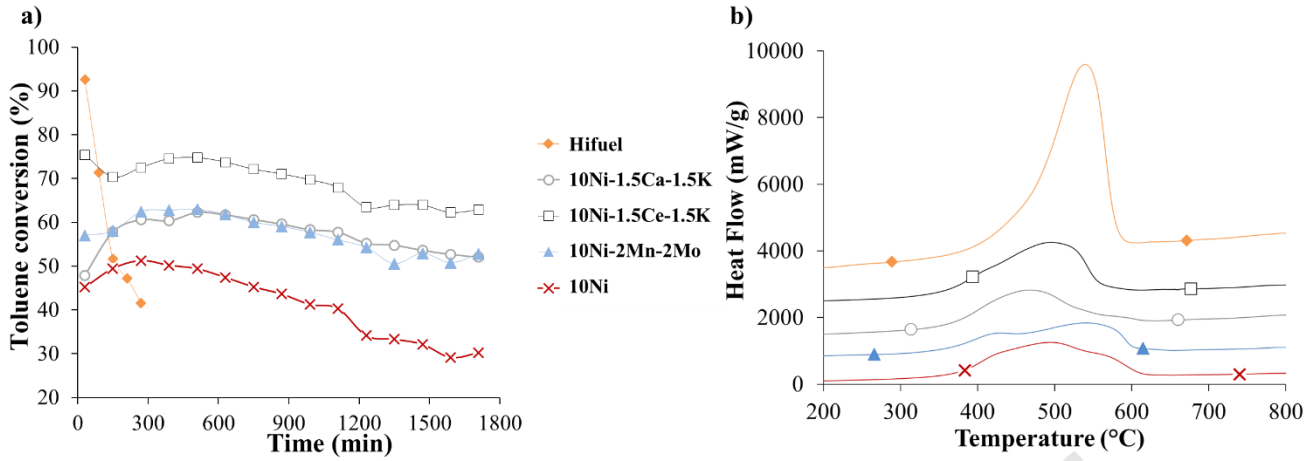

Figure 5: (a) Toluene conversion as a function of time for long-term experiments and (b) DSC curves after long-term catalytic experiments. Note: for Hifuel sample, the experiment was switched off after 300 min.

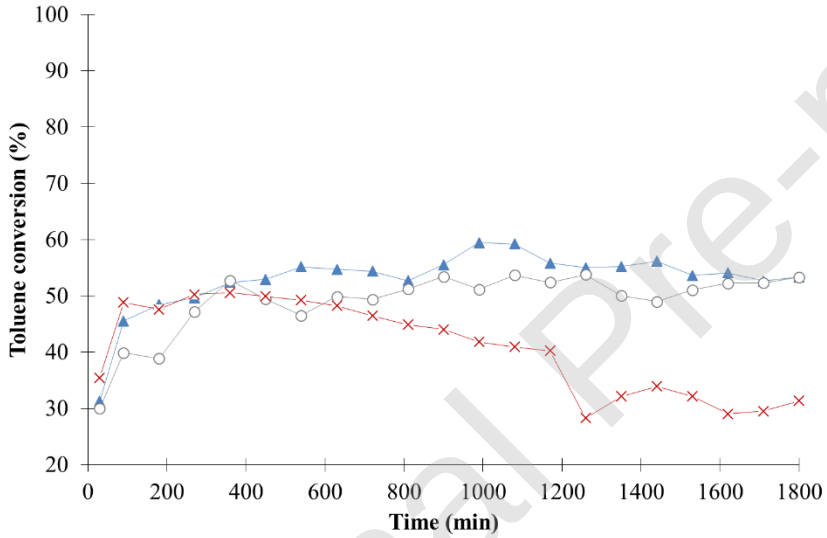

Figure 6: Toluene conversion as a function of time for (×) 10Ni, (▲) 10Ni-2Mn-2Mo, and (○) 10Ni-1.5Ca-1.5K samples after regeneration under air.

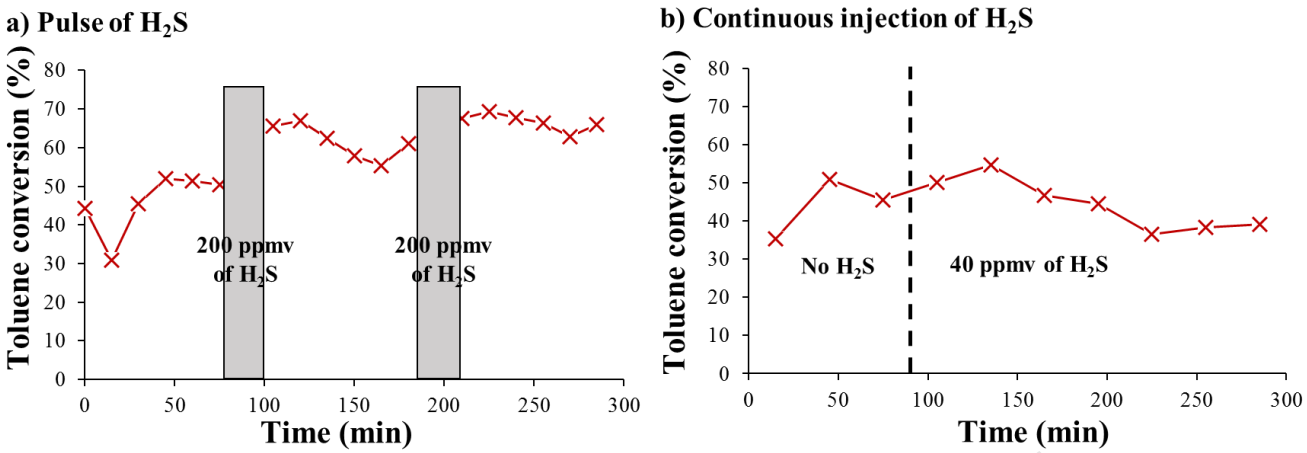

Figure 7: Toluene conversion as a function of time in sulphidic conditions for 10Ni sample: (a) pulses of 200 ppmv of H_2S and (b) continuous flow of 40 ppmv of H_2S.

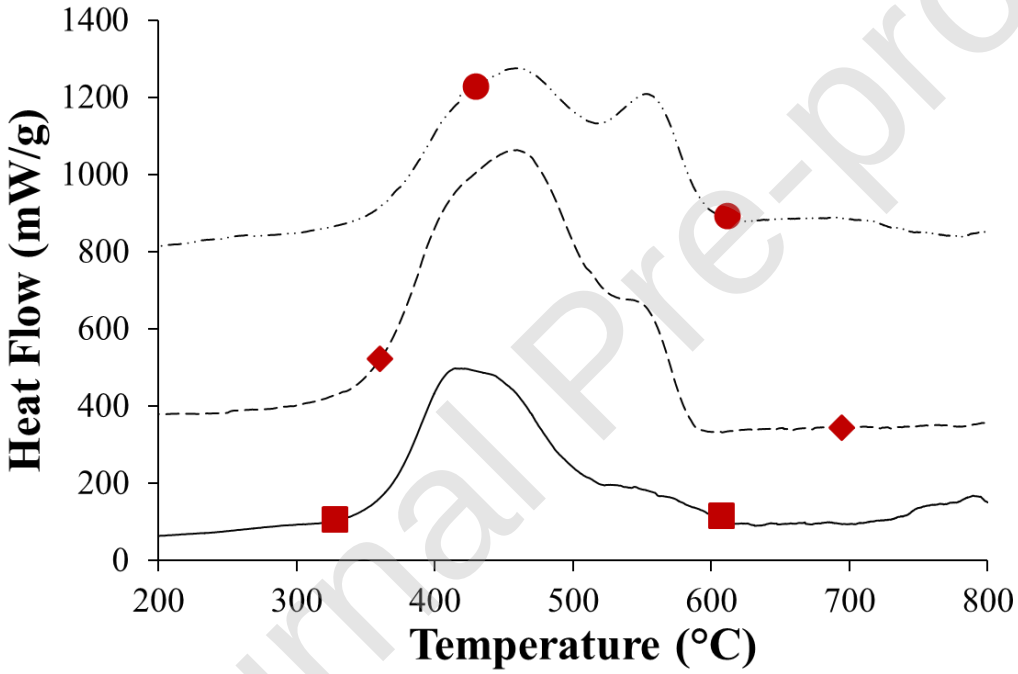

Figure 8: DSC curves after catalytic experiments performed in presence of H_2S: (■) 10Ni (classic experiment without H_2S), (♦) 10Ni-Pulse, (●) 10Ni-Continuous.

Table 1: Global reactions between a metallic active site (M) and H_2S; and following regeneration with H_2, H_2O or O_2

Reaction	Name of reaction	Reaction n°
$MO_x + x.H_2S \rightarrow MS_x + x.H_2O$	Reduction and poisoning	(1)
$M + x.H_2S \rightarrow MS_x + x.H_2$	Poisoning	(2)
$MS_x + x.H_2O \rightarrow MO_x + x.H_2S$	Regeneration by H_2O	(3)
$MS_x + x.H_2 \rightarrow M + x.H_2S$	Regeneration by H_2	(4)

$MS_x + (3.x/2).O_2 \rightarrow MO_x + x.SO_2$ Regeneration by O_2 (5)

Table 2: Composition and textural properties of samples

Sample	Theoretical composition (wt. %)	Actual composition (wt. %)	S_{BET} (m^2/g)	V_p (cm^3/g)	V_{DR} (cm^3/g)	V_{Hg} (cm^3/g)
10Ni	90.0 Al_2O_3 / 10.0 Ni	90.5 Al_2O_3 / 9.5 Ni	240	0.3	0.08	<0.1
10Ni-2Mn-2Mo	86.0 Al_2O_3 / 10.0 Ni / 2.0 Mn / 2.0 Mo	85.3 Al_2O_3 / 10.9 Ni / 1.7 Mn / 2.1 Mo	245	0.3	0.08	<0.1
10Ni-1.5Ca-1.5K	87.0 Al_2O_3 / 10.0 Ni / 1.5 Ca / 1.5 K	85.8 Al_2O_3 / 11.0 Ni / 1.5 Ca / 1.7 K	255	0.3	0.08	<0.1
10Ni-1.5Ce-1.5K	87.0 Al_2O_3 /10.0 Ni / 1.5 Ce / 1.5 K	85.5 Al_2O_3 / 11.1 Ni / 1.7 Ce / 1.7 K	245	0.3	0.08	<0.1
Hifuel	-	67.4 Al_2O_3 / 16.0 Ni / 16.3 CaO / 0.1 SiO_2 / 0.1 MgO / 0.1 Na_2O	20	0.08	0.008	0.2

S_{BET}: specific surface area determined from nitrogen adsorption-desorption isotherms and using the Brunauer-Emmet-Teller theory; V_p: porous volume determined from nitrogen adsorption-desorption isotherms at saturation pressure; V_{DR}: microporous volume determined from Dubinin-Raduskevitch theory; V_{Hg}: macroporous volume measured by mercury porosimetry.

Table 3: Ni particles size of samples after reduction and after TPR measurements

Sample	After reduction			After TPR		
	d_{TEM} (nm)	σ_{TEM} (nm)	d_{XRD} (nm)	d_{TEM} (nm)	σ_{TEM} (nm)	d_{XRD} (nm)
10Ni	12	4	12	30	9	23
10Ni-2Mn-2Mo	11	3	11	25	5	21
10Ni-1.5Ca-1.5K	10	9	12	33	11	27
10Ni-1.5Ce-1.5K	9	3	11	33	10	25

Hifuel	26	15	23	32	26	34

d_{TEM}: metallic particles size median; σ_{TEM}: standard deviation; d_{XRD} : metallic nickel crystallites size estimated by XRD.

Table 4: Metallic particles size, metal alloy phases and catalytic performances of catalysts during long-term experiments. Operating conditions: T = 650 °C; t = 30 h; 24,000 ppmv of toluene; $GHSV$ = 5000 h^{-1}

Sample	Particles size			Metal phase	Catalytic performances				
	d_{TEM} (nm)	σ_{TEM} (nm)	d_{XRD} (nm)		C_T (%)	C_{CH4} (%)	S_B (%)	Coke (g_{Carbon}/g_{Cata})	Fil. carbon
10Ni	12	4	12	Ni	50 → 30	12 → 14	12 → 7	0.20	+
10Ni-2Mn-2Mo	12	2	10	$Ni_{0.97}Mo_{0.03}$	59 → 52	11 → 10	7 → 7	0.19	+
10Ni-1.5Ca-1.5K	12	5	12	Ni	59 → 53	10 → 14	5 → 4	0.19	+
10Ni-1.5Ce-1.5K	16	7	12	Ni	72 → 63	13 → 8	4 → 3	0.28	+
Hifuel	30	16	25	Ni	90 → 42	-3 → -3	10 → 58	0.96	+++

Note: Test with Hifuel sample stopped at t = 300 min because of a too high pressure (P > 3 atm)

d_{TEM}: metallic particles size median; σ_{TEM}: standard deviation; d_{XRD}: metallic crystallites size estimated by XRD; C_T: conversion of toluene; S_B: selectivity in benzene, C_{CH4}: conversion of methane; *Coke*: carbon deposit amount after 30 h of test measured by TG-DSC. For all samples, except Hifuel sample, the catalytic activity values (C_T, S_B, C_{CH4}) were determined by making an average of the values between 60-300 min, and between 1500-1740 min. For Hifuel sample, the average values were calculated on the first 5 injections and the last 5 injections.

Table 5: Ni particles size and catalytic performances of 10Ni sample with pulses of 200 ppmv of H_2S or with a continuous injection of 40 ppmv of H_2S. Operating conditions: T = 650 °C; t = 5 h; 24,000 ppmv of toluene; $GHSV$ = 5000 h^{-1}

Sample	Ni particles size			Catalytic performances				
	d_{TEM} (nm)	σ_{TEM} (nm)	d_{XRD} (nm)	C_T (%)	C_{CH4} (%)	S_B (%)	Coke (g_{Carbon}/g_{Cata})	Fil. carbon
10Ni (standard test)	11	3	12	51	10	15	0.10	No
10Ni-Pulse	12	6	11	49→63	7 → 10	17→7	0.14	+
10Ni-Continuous	14	8	12	48→37	7→1	12→10	0.11	+

d_{TEM}: metallic particles size median; σ_{TEM}: standard deviation; d_{XRD}: metallic crystallites size estimated by XRD; C_T: conversion of toluene; S_B: selectivity in benzene, C_{CH4}: conversion of methane; *Coke*: carbon deposit amount after 5 h of test measured by TG-DSC. The catalytic activity values (C_T, S_B, C_{CH4}) were the average values calculated on the first 5 injections and the last 5 injections.